Inorganic Chemistry
Article

Inorg. Chem. **2010**, *49*, 2889–2900 **2889**
DOI: 10.1021/ic902427r

Photobiological Activity of Ru(II) Dyads Based on (Pyren-1-yl)ethynyl Derivatives of 1,10-Phenanthroline

Susan Monro,[†] John Scott,[†] Abdellatif Chouai,[‡] Richard Lincoln,[†] Ruifa Zong,[‡] Randolph P. Thummel,*[,‡] and Sherri A. McFarland*[,†]

[†]*Department of Chemistry, Acadia University, Wolfville, NS B4P 2R6, Canada and* [‡]*Department of Chemistry, University of Houston, Houston, Texas 77204−5003*

Received December 7, 2009

Several mononuclear Ru(II) dyads possessing 1,10-phenanthroline-appended pyrenylethynylene ligands were synthesized, characterized, and evaluated for their potential in photobiological applications such as photodynamic therapy (PDT). These complexes interact with DNA via intercalation and photocleave DNA in vitro at submicromolar concentrations when irradiated with visible light ($\lambda_{irr} \geq 400$ nm). Such properties are remarkably sensitive to the position of the ethynylpyrenyl substituent on the 1,10-phenanthroline ring, with 3-substitution showing the strongest binding under all conditions and causing the most deleterious DNA damage. Both dyads photocleave DNA under hypoxic conditions, and this photoactivity translates well to cytotoxicity and photocytotoxicity models using human leukemia cells, where the 5- and 3-substituted dyads show photocytotoxicity at 5−10 μM and 10−20 μM, respectively, with minimal, or essentially no, dark toxicity at these concentrations. This lack of dark cytotoxicity at concentrations where significant photoactivity is observed emphasizes that agents with strong intercalating units, previously thought to be too toxic for phototherapeutic applications, should not be excluded from the arsenal of potential photochemotherapeutic agents under investigation.

1. Introduction

Traditionally, dyad-type molecules have piqued curiosity owing to their potential in photonic-based applications. Specifically, several dyads assembled from Ru(II) polypyridyl complexes have been shown to display some of the longest lifetimes (> 150 μs) observed for ruthenium-based coordination complexes due to excited-state equilibrium that is established between the two components of the dyad, namely, the Ru(II) diimine complex and a pendant polycyclic aromatic hydrocarbon.[1] The synergistic communication between these constituent components, while interesting from a theoretical perspective, may prove to have far-reaching consequences not only in applications such as supramolecular chemistry but also in the area of photobiology, particularly in the design of phototherapeutic agents. The planar appendage provides a handle for intercalative binding to DNA,[2−6] positioning the complex for enhanced reactivity toward DNA. Increased photoreactivity toward DNA has been observed for Ru(II) complexes containing the intercalating dppz (dipyrido[3,2-*a*:2′,3′-*c*]phenazine) ligand and its derivatives[3] and more recently for dirhodium(II) complexes that incorporate the dppz ligand, which photocleave DNA and exhibit photocytotoxicity toward certain cancer cell lines.[7] Moreover, the dyad motif positions the lowest-energy π*-acceptor ligand at a relatively long distance from the Ru(II) core, which profoundly increases the charge-separation that can be achieved in conventional ^{3}MLCT excited states. This increased charge-separation may lead to longer excited-state lifetimes and reactive excited states that are capable of oxidizing DNA without the need for an external electron acceptor.[8] Such states are of interest in the development of photosensitizers that absorb low-energy light and function in the absence of oxygen. The ability to damage DNA under hypoxic conditions with photoactivation by visible light would be a first-step toward the development of ruthenium-based drugs for use in photobiological applications such as photodynamic therapy (PDT).

*To whom correspondence should be addressed. E-mail: sherri.mcfarland@acadiau.ca (S.A.M.), thummel@uh.edu (R.P.T.).

(1) McClenaghan, N. D.; Leydet, Y.; Maubert, B.; Indelli, M. T.; Campagna, S. *Coord. Chem. Rev.* **2005**, *249*, 1336–1350.
(2) Zeglis, B. M.; Pierre, V. C.; Barton, J. K. *Chem. Commun.* **2007**, 4565–4579.
(3) Delaney, S.; Pascaly, M.; Bhattacharya, P. K.; Han, K.; Barton, J. K. *Inorg. Chem.* **2002**, *41*, 1966–1974.
(4) Erkkila, K. E.; Odom, D. T.; Barton, J. K. *Chem. Rev.* **1999**, *99*, 2777–2796.
(5) Holmlin, R. E.; Stemp, E. D.; Barton, J. K. *Inorg. Chem.* **1998**, *37*, 29–34.
(6) Jenkins, Y.; Friedman, A. E.; Turro, N. J.; Barton, J. K. *Biochemistry* **1992**, *31*, 10809–10816.
(7) Angeles-Boza, A. M.; Bradley, P. M.; Fu, P.; Wicke, S. E.; Bacsa, J.; Dunbar, K. R.; Turro, C. *Inorg. Chem.* **2004**, *43*, 8510–8519.
(8) Stemp, E.; Arkin, M. R.; Barton, J. K. *J. Am. Chem. Soc.* **1997**, *119*, 2921–2925.

Published on Web 02/10/2010

Chart 1. Diimine Ligands Linked to Pyrene

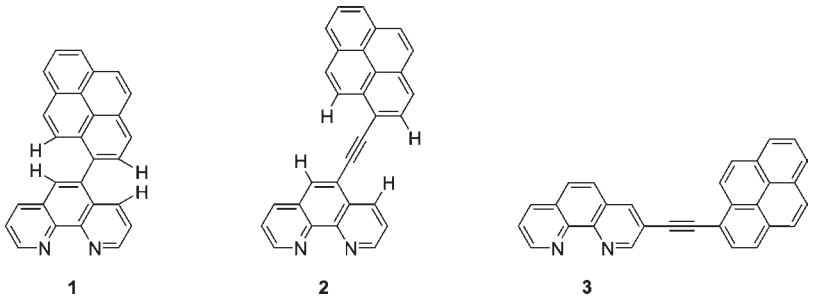

1 2 3

Diimine ligands linked directly to pyrene have been prepared, and the photophysics of their Ru(II) complexes have been studied carefully by Schmehl,[9,10] Castellano,[11] Schlüter[12] and co-workers. When the pyrene is directly linked to 2,2′-bipyridine (bpy) or 1,10-phenanthroline (phen), conformational interaction of hydrogens near the linkage cause non-planarity of the system that interferes substantially with electronic communication between the two halves of the dyad (**1**; Chart 1). This problem can be alleviated by using an ethynyl bridge in place of the direct covalent C−C linkage.[13−18] This ethynyl bridge maintains the rigidity and linearity of a C−C bond while moving the dyad units apart such that conformational interactions assume a less important role. Additionally, the cylindrical symmetry of the triple bond provides good conjugative interaction between the ligand and the pyrene residue regardless of the relative dihedral orientation of their respective planar π-networks. This situation is illustrated for 1,10-phenanthroline substituted at the 5-position with either a 1-pyrenyl (**1**)[11,19] or a (pyren-1-yl)ethynyl (**2**) group. We have recently prepared dyad ligands **2** and **3** and their corresponding heteroleptic complexes $[Ru(\mathbf{2})(bpy\text{-}d_8)_2]^{2+}$ (**7**) and $[Ru(\mathbf{3})(bpy\text{-}d_8)_2]^{2+}$ (**8**). In this paper we discuss the synthesis and characterization of these systems, including their photophysical and electrochemical properties, as well as their interactions with DNA. We also explore the cytotoxicity and photocytotoxicity of **7** and **8** toward human leukemia cells (Chart 2).

Chart 2. Ruthenium(II) Complexes of Ethynylpyrene-Linked Diimine Ligands

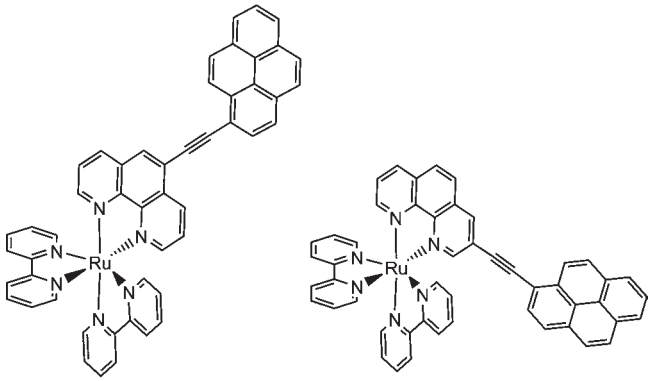

7 8

2. Experimental Procedures

2.1. Materials. Acetic acid, acridine orange, agarose, Optima-grade acetonitrile, ethylenediaminetetraacetic acid (EDTA), ethidium bromide, ethanol, gentamicin (50 mg mL^{-1}, in sterile-filtered water), Hoechst 33258, 4-morpholinepropanesulfonic acid (MOPS), trishydroxymethylaminomethane (Tris base), Tris/HCl, trypan blue (0.4% w/v, sterile-filtered), and sodium chloride were purchased from Sigma-Aldrich and used as received without further purification. Distilled, deionized water (ddH_2O) was obtained from a Millipore system. Calf-thymus DNA (activated type XV) was purchased from Sigma and reconstituted with 40 mM MOPS (pH 7.5) overnight at room temperature following sonication. The concentration of the resulting DNA solution was calculated from its absorbance (A_{260}) using $\epsilon = 12824\ M^{-1}\ cm^{-1}$ (base pairs), and purity was estimated by relative absorption at 260 and 280 nm ($A_{260}/A_{280} \sim 1.8$). Plasmid pUC19 DNA was purchased from New England BioLabs and transformed using NovaBlue Singles Competent Cells purchased from Novagen. Transformed pUC19 was purified using the QIAprep Spin Miniprep Kit purchased from Qiagen (yield ~62 μg of plasmid DNA per 20 mL culture). Supercoiled p*Des*R3 plasmid was a derivative of pET28a containing the *desR* gene[20] and was used in the present study because of its increased GC content.[21] Characterized fetal bovine serum (FBS) and Iscove's Modified Dulbecco's Medium (IMDM) supplemented with 4 mM L-glutamine were purchased from Fisher Scientific, and human promyelocytic leukemia cells (HL60) were supplied by the American Type Culture Collection (ATCC CCL-240). Prior to use FBS was divided into 40 mL aliquots that were heat inactivated (30 min, 55 °C) and subsequently stored at −10 °C. Acetonitrile used for cyclic voltammetry experiments was dried by reflux over CaH_2 and distilled under argon prior to use. 3-Bromo-1,10-phenanthroline,[22,23]

(9) Del Guerzo, A.; Leroy, S.; Fages, F.; Schmehl, R. H. *Inorg. Chem.* **2002**, *41*, 359–366.
(10) Simon, J. A.; Curry, S. L.; Schmehl, R. H.; Schatz, T. R.; Piotrowiak, P.; Jin, X.; Thummel, R. P. *J. Am. Chem. Soc.* **1997**, *119*, 11012–11022.
(11) Tyson, D. S.; Bialecki, J.; Castellano, F. N. *Chem. Commun.* **2000**, 2355–2356.
(12) Beinhoff, M.; Weigel, W.; Jurczok, M.; Rettig, W.; Modrakowski, C.; Brüdgam, I.; Hartl, H.; Schlüter, A. D. *Eur. J. Org. Chem.* **2001**, 3819–3829.
(13) Harriman, A.; Hissler, M.; Khatyr, A.; Ziessel, R. *Chem. Commun.* **1999**, 735–736.
(14) Kozlov, D. V.; Tyson, D. S.; Goze, C.; Ziessel, R.; Castellano, F. N. *Inorg. Chem.* **2004**, *43*, 6083–6092.
(15) Goze, C.; Kozlov, D. V.; Tyson, D. S.; Ziessel, R.; Castellano, F. N. *New J. Chem.* **2003**, *27*, 1679–1683.
(16) Goze, C.; Kozlov, D. V.; Castellano, F. N.; Suffert, J.; R. Ziessel, R. *Tetrahedron Lett.* **2003**, *44*, 8713–8716.
(17) Khatyr, A.; R. Ziessel, R. *Tetrahedron Lett.* **2002**, *43*, 7431–7434.
(18) Hissler, M.; Harriman, A.; Khatyr, A.; Ziessel, R. *Chem. Eur. J.* **1999**, *5*, 3366–3381.
(19) Tyson, D. S.; Henbest, K. B.; Bialecki, J.; Castellano, F. N. *J. Phys. Chem. A* **2001**, *105*, 8154–8161.
(20) Xue, Y.; Zhao, L.; Liu, H.; Sherman, D. H. *Proc. Natl. Acad. Sci. U.S.A.* **1998**, *95*, 12111–12116.
(21) Sáez Díaz, R. I.; Regourd, J.; Santacroce, P. V.; Davis, J. T.; Jakeman, D. L.; Thompson, A. *Chem. Commun.* **2007**, 2701–2703.
(22) Tzalis, D.; Tor, Y.; Failia, S.; Siegel, J. S. *Tetrahedron Lett.* **1995**, *36*, 3489–3490.
(23) Connors, P. J.; Tzalis, D.; Dunnick, A. L.; Tor, Y. *Inorg. Chem.* **1998**, *37*, 1121–1123.

5-bromo-1,10-phenanthroline,[24,25] and $[Ru(bpy\text{-}d_8)_2Cl_2]\text{-}2H_2O$[27] were prepared according to known procedures. 1-Ethynylpyrene was purchased from Aldrich and used without further purification.

2.2. Instrumentation. NMR spectra were recorded at 300 MHz for ^1H and referenced to tetramethylsilane (TMS) in $CDCl_3$ and to the residual solvent peak in CD_3CN. Electronic spectra were measured on Jasco V-530 and Perkin-Elmer Lambda 3B spectrophotometers. The Jasco V-530 spectrophotometer was equipped with a ETC-505T Peltier temperature controller for DNA melting experiments. Fluorescence spectra were obtained on PTI Quantamaster and Perkin-Elmer LS-50 luminescence spectrometers. The PTI Quantamaster was equipped with a standard R928 PMT for measuring conventional emission (< 900 nm) and a Hamamatsu R5509−42 NIR PMT for measuring near infrared (NIR) emission (< 1400 nm). Cyclic voltammetry was carried out in a conventional three-electrode cell with a BAS-27 potentiostat and a Houston Instruments model 100 X-Y recorder according to a previously described procedure.[27] Mass spectra were obtained on a Hewlett-Packard 5989B mass spectrometer (59987A electrospray) using atmospheric pressure ionization at 160 °C. Elemental analyses were performed by National Chemical Consulting, P.O. Box 99, Tenafly, NJ 07670. Melting points were measured on a Hoover capillary melting point apparatus and are not corrected. DNA photocleavage experiments were carried out in a Luzchem LZC-4X photoreactor equipped with both side- and top-illumination with LZC-420 bulbs (exposure standards available from Luzchem). Ethidium bromide-stained agarose gels were imaged using the Gel Doc-It imaging system from UVP or with a Kodak EasyShare C330 digital camera with the GNU Image Manipulation Program (GIMP). Viscosity measurements were made using the model E120 50 semimicro viscometer purchased from Cannon-Manning. Cellular counting and imaging was carried out using a Nikon Eclipse TE2000-U inverted light microscope in phase-contrast mode or epi-fluorescence mode (G-2A epi-fluorescence filter block). Manual cell counting was done using a Neubauer hemocytometer (Hausser Scientific).

2.3. Synthesis and Characterization. 5-(Pyren-1′-yl)ethynyl-1,10-phenanthroline (2). To a pressure tube were added 5-bromo-1,10-phenanthroline (**5**, 250 mg, 0.97 mmol), 1-ethynylpyrene (**4**, 328 mg, 1.45 mmol), $[Pd(PPh_3)_4]$(167 mg, 0.144 mmol), and *n*-propylamine (40 mL). Ar was bubbled through the solution for 10 min, and the vessel then sealed with a Teflon stopcock and heated at 80 °C for 2 days. After cooling, the precipitate was filtered, washed with H_2O (10 mL), MeOH (10 mL) and CH_2Cl_2 (10 mL), dried and chromatographed on SiO_2, eluting with CH_2Cl_2/MeOH (99:1) to give **2** (285 mg, 73%) as a yellow solid, mp 133−135 °C; ^1H NMR ($CDCl_3$): δ 9.31 (dd, H9, J = 4.2, 1.5, Hz), 9.25 (dd, H2, J = 4.2, 1.5 Hz), 9.09 (dd, H4, J = 8.1, 1.5 Hz), 8.77 (d, H2′ or H10′, J = 9 Hz), 8.37−8.05 (overlapping m, 10 H), 7.84 (dd, H3 or H8, J = 8.1, 4.2 Hz), 7.71, (dd, H3 or H8, J = 8.1, 4.5 Hz); ^{13}C NMR could not be obtained because of poor solubility; MS: m/z 405.3 (100%, (M + 1); Anal. Calcd for $C_{30}H_{16}N_2\cdot 0.20H_2O$: C, 87.17; H, 4.12; N, 6.80. Found: C, 87.48; H, 3.37; N, 6.59.

3-(Pyren-1′-yl)ethynyl-1,10-phenanthroline (3). Following the procedure described for **2**, a mixture of 3-bromo-1,10-phenanthroline[22,23] (**6**, 100 mg, 0.39 mmol), 1-ethynylpyrene (**4**, 131 mg, 0.58 mmol), $[Pd(PPh_3)_4]$(67 mg, 0.058 mmol), and *n*-propylamine (15 mL) was heated at 80 °C for 2 days to give **3** (125 mg, 79%) as a brownish solid, mp 168−172 °C: ^1H NMR ($CDCl_3$): δ 9.45 (d, H2, J = 1.8 Hz), 9.24 (dd, H9, J = 4.2, 1.8 Hz), 8.71 (d, H2′ or H10′, J = 9 Hz), 8.54 (d, H4, J = 1.8 Hz), 8.30−8.03 (overlapping m, 9 H), 7.82 (s, H5 and H6), 7.66 (dd, H8, J = 8.1, 4.5 Hz); ^{13}C NMR could not be obtained because of poor solubility; MS: m/z 405.4 (100%, (M + 1); Anal. Calcd for $C_{30}H_{16}N_2\cdot 0.5\ H_2O$: C, 86.08; H, 3.89; N, 6.65. Found: C, 86.29; H, 3.54; N, 6.71.

$[Ru(2)(bpy\text{-}d_8)_2](PF_6)_2$ (7). A mixture of **2** (40.5 mg, 0.100 mmol) and *cis*-$[Ru(bpy\text{-}d_8)_2Cl_2]\text{-}2H_2O$ (59.0 mg, 0.110 mmol) in absolute EtOH (40 mL) was refluxed under Ar for 24 h. After cooling, excess NH_4PF_6 (aq) was added, and the mixture was stirred for 20 min. The solvent was evaporated, and the crude product was chromatographed on SiO_2, eluting with CH_2Cl_2/MeOH (99:1) to afford **7** as an orange solid (74 mg, 66%), mp > 280 °C: ^1H NMR (CD_3CN): δ 9.11 (d, H4, J = 8.4 Hz), 8.73 (d, H2′ or H10′, J = 9 Hz), 8.60 (s, H6), 8.59 (d, H7, J = 7.5 Hz), 8.4−8.03 (overlapping m, 10 H), 7.88 (dd, H3 or H8, J = 8.4, 5.1 Hz), 7.77 (dd, H3 or H8, J = 8.1, 5.1 Hz); MS: m/z 416.6 (100%, $(M-2PF_6)/2$).

$[Ru(3)(bpy\text{-}d_8)_2](PF_6)_2$ (8). A mixture of **3** (40.5 mg, 0.100 mmol) and *cis*-$[Ru(bpy\text{-}d_8)_2Cl_2]\text{-}2H_2O$ (59.0 mg, 0.110 mmol) in absolute EtOH (35 mL) was refluxed under Ar for 20 h. After cooling, excess NH_4PF_6 (aq) was added, and the mixture was stirred for 20 min. The solvent was evaporated, and the crude product was chromatographed on SiO_2, eluting with CH_2Cl_2/MeOH (99:1) to afford **8** as a reddish solid (75 mg, 67%), mp > 280 °C: ^1H NMR (CD_3CN): δ 8.91 (s, H4), 8.64 (d, H2′ or H10′, J = 8.1 Hz), 8.52 (d, H7, J = 9 Hz), 8.41−8.10 (overlapping m, 12 H), 7.76 (dd, H8, J 8.1, 5.1 Hz); MS: m/z 417 (100%, $(M-2PF_6)/2$).

2.4. Methods. 2.4.1. DNA Binding by UV−vis. Optical titrations were carried out on 0.5−2 mL solutions of the dyads with increasing amounts of calf thymus or herring sperm DNA to give [DNA bases]/[Ru] between 0.1 and 10. DNA was added in 1−5 μL increments to solutions of compound (10 μM) in 10 mM MOPS, 10 mM MOPS with 50 mM NaCl, 5 mM Tris-HCl, or 5 mM Tris-HCl with 50 mM NaCl at pH 7.5. The dilution of metal complex concentration at the end of each titration, although negligible, was accounted for in the binding constant analyses. The DNA binding constant (K_b) was obtained from fits of the titration data to eq 1,[28,29] where $b = 1 + K_bC_t + K_b[DNA]_t/2s$, C_t and $[DNA]_t$ represent the total dyad and DNA concentrations, respectively, s is the binding site size, and ϵ_a, ϵ_f, and ϵ_b represent the molar extinction coefficients of the apparent, free, and bound metal complexes, respectively. ϵ_f was calculated at 414 nm for **7** and 412 nm for **8** before the addition of DNA, and ϵ_a was determined at these wavelengths after each addition of DNA. The value of ϵ_b was determined from the plateau of the DNA titration, where addition of DNA did not result in any further decrease in the absorption signal. Detailed fits of the titration data were obtained using both Kaleidagraph and Gnuplot.

$$\frac{\epsilon_a - \epsilon_f}{\epsilon_b - \epsilon_f} = \frac{b - (b^2 - 2K_b^2C_t[DNA]_t/s)^{1/2}}{2K_bC_t} \qquad (1)$$

DNA melting curves were constructed by measuring the absorbance (A_{260}) of a 2 mL, 25 μM DNA solution (40 mM MOPS, pH 7.5) as a function of temperature (20−100 °C) in the absence and presence of compound (5 μM). Solutions of DNA and compound for melting experiments were allowed to equilibrate for 30 min at 25 °C prior to measurement. The ETC-505T temperature controller was cooled with ice water (4 °C) using a fish-aquarium pump, and a stream of argon gas was supplied via the gas inlet valve to the sample compartment to prevent condensation on the cuvette windows during variable-temperature experiments.

(24) Hissler, M.; Connick, W. B.; Geiger, D. K.; McGarrah, J. E.; Lipa, D.; Lachicotte, R. J.; Eisenberg, R. *Inorg. Chem.* **2000**, *39*, 447–457.
(25) Mlochowski, J. *Roczniki Chem., Ann. Soc. Chim. Polonorum* **1974**, *48*, 2145.
(26) Ziessel, R.; Stroh, C. *Tetrahedron Lett.* **2004**, *45*, 4051–4055.
(27) Goulle, V.; Thummel, R. P. *Inorg. Chem.* **1990**, *29*, 1767–1772.
(28) Carter, M. T.; Rodriguez, M.; Bard, A. J. *J. Am. Chem. Soc.* **1989**, *111*, 8901–8911.
(29) Kalsbeck, W. A.; Thorp, H. H. *J. Am. Chem. Soc.* **1993**, *115*, 7146–7151.

2.4.2. DNA Binding by Viscosity. Relative viscosity measurements were made by charging the Cannon−Manning semimicro viscometer with varying concentrations of compound (7.5−45 μM) dissolved in 10 mM MOPS (pH 7.5) containing 150 μM (base pairs) calf thymus DNA, giving [compound]/[DNA bp] ratios of 0.05−0.3. An identical solution without the sample compound was used to reference each measurement. Trials were performed in triplicate, and the viscometer was thoroughly rinsed with ddH_2O and 10 mM MOPS between samples followed by removal of all trace droplets under reduced pressure. Samples were loaded, following equilibration for 30 min at 25 °C prior to measurement, with the viscometer in an inverted position by immersing tube N in the sample while applying suction to tube L with a 3-way safety bulb. When the sample approached mark G, the viscometer was returned to an upright position and secured in its commercial holder at 25 °C. The efflux time of the sample was measured as the time it took for the meniscus to move between the timing notches, mark E to mark F. Relative viscosity for a given sample was calculated as $(\eta/\eta_o)^{1/3}$, where η is the efflux time of the sample solution with DNA and η_o is the efflux time of a solution containing only DNA. Ethidium bromide and Hoechst 33258 were used as standards.

2.4.3. Photocleavage Titrations. DNA photocleavage experiments were performed according to a general plasmid DNA assay[30,31] with 20 μL total sample volumes in 0.5 or 1.5 mL microfuge tubes containing transformed pUC19 plasmid (200 ng, >95% Form I) in 10 mM MOPS buffer and 100 mM NaCl, pH 7.4. DNA (1−5 μL) was delivered to the assay tubes as a solution in 10 mM Tris-Cl (pH 8.5) and diluted with MOPS (pH 7.5, final concentration 10 mM) and NaCl (final concentration 100 mM). Solutions of complexes **7** or **8** were added to give the desired concentration, and the reaction mixtures were diluted to a final volume of 20 μL, when necessary, with ddH_2O. Complexes were dissolved initially in acetonitrile (2 μM stock solutions), and all subsequent dilutions were made with ddH_2O where final assay tubes contained <1% acetonitrile. For concentration-based assays, samples (no pre-incubation period) were irradiated in air for 30 min with 420 nm light inside a photoreactor (Luzchem LZC-4X). Where irradiation of deoxygenated samples was required, argon was bubbled through the solutions for 15 min prior to irradiation under a positive pressure of argon. All samples were quenched by the addition of gel loading buffer (4 μL), loaded onto 1% agarose gels containing ethidium bromide (0.75 μg mL^{-1}), and electrophoresed for 30 min at 8−12 V cm^{-1} in 1X TAE (40 mM Tris-acetate, 1 mM EDTA, pH 8.2). The bands were visualized with UV-transillumination (UVP transilluminator) and quantified using the Gel Doc-It Imaging system (UVP) or GNU Image Manipulation Program (GIMP).

2.4.4. Cell Culture. HL-60 human promyelocytic leukemia cells (ATCC CCL-240) were cultured at 37 °C under 5% CO_2 in Hyclone's IMDM, supplemented with 20% FBS and 25 μg mL^{-1} gentamycin sulfate, and were passaged 3−4 times per week according to standard aseptic procedures. Cultures were started at 200,000 cells mL^{-1} in 25 cm^2 tissue culture flasks and were subcultured before growth reached 750,000 cells mL^{-1} to avoid senescence associated with prolonged high cell density. Complete media was prepared in 200 mL portions as needed by combining IMDM (160 mL), FBS (40 mL, pre-aliquoted and heat inactivated), and gentamicin sulfate (100 μL of 50 mg mL^{-1} stock solution) in a 250 mL Millipore vacuum stericup (0.22 μm) and filtering.

2.4.5. Cytotoxicity and Photocytotoxicity Assays. HL-60 cells growing in log phase were transferred (typically 25 μL aliquots) to 96-well tissue-culture plates (Corning Costar, Acton, MA) containing culture medium either with or without varying concentrations of complex to give final volumes in the culture wells of 100 μL and 10,000−20,000 cells. Solutions of complex in complete media were prepared in 1 mL portions, where acetonitrile from the initial complex stock solution was <0.5% v/v, and sterile-filtered in 3 mL syringes equipped with 0.22 μm Nalgene filters. Plates were incubated at 37 °C under 5% CO_2 for 30 min prior to exposure to 420 nm light in a Luzchem photoreactor for 30 min; dark controls were incubated under identical conditions in the dark. Dark controls, or cytotoxicity (CT) assays, refer to assays that include metal complex but were not exposed to light, and light controls refer to light-exposed assays that did not contain metal complex. Photocytotoxicity (PCT) assays contained metal complex and were exposed to light. Cell counts and viability staining were carried out immediately and at ~24 h following light exposure. Manual counts were performed on 25 μL 1:1 mixtures of assay culture and trypan blue solution in a Neubauer hemocytometer viewed under an inverted light microscope in phase-contrast mode (4X objective, 60X total magnification). Under these conditions, viable cells appeared bright white, and non-viable cells were blue. All experiments were carried out in triplicate, and the graphed data is the average of three trials.

2.4.6. Viability Staining. Viability was established according to a published protocol,[32,33] whereby a 100X stock solution of ethidium bromide/acridine orange (EB/AO) was prepared by dissolving ethidium bromide (50 mg) and acridine orange (15 mg) in 95% ethanol (1 mL) and diluting 1/50 with ddH_2O. The 100X solution was divided into 1 mL aliquots and stored at −20 °C. A 1X working solution was made by thawing a 1 mL aliquot of the 100X stock solution and diluting 1/100 with phosphate-buffered saline. The working solution was stored in an amber bottle at 4 °C for up to 1 month. For cellular viability staining, an aliquot of cell suspension was adjusted to $1-5 \times 10^6$ cells mL^{-1} in phosphate-buffered IMDM. A 25 μL aliquot of this cell suspension was mixed with 1X EB/AO staining solution (25 μL) in a microfuge tube; a 25 μL aliquot of this cell-stain mixture was transferred to a hemocytometer and viewed under a Nikon Eclipse TE2000-U inverted light microscope operating in epi-fluorescence mode (10X or 40X objective, 150X or 600X total magnification). Under these conditions, viable cells took up AO and excluded EB, resulting in only green fluorescence with UV-excitation. Non-viable cells (apoptotic or necrotic) assimilated EB and fluoresced red with green excitation, overwhelming any green fluorescence from AO. Apoptotic cells were discerned from the formation of smaller, apoptotic bodies that fluoresced red.

3. Results and Discussion

3.1. Synthesis and Characterization. Following a modified procedure described by Eisenberg and co-workers,[24,25] 5-bromo-1,10-phenanthroline (**5**) was synthesized in 72% yield by treating 1,10-phenanthroline with bromine and H_2SO_4 in a sealed tube at 135 °C for 23 h. The 5-(pyren-1′-yl)ethynyl-1,10-phenanthroline (**2**) was prepared in 73% yield by heating a mixture of **5** and a slight excess of 1-ethynylpyrene (**4**) with 15 mol % $[Pd(PPh_3)_4]$ and *n*-propylamine as both the base and the solvent at 80 °C for 2 days.

Following a procedure recently described by Tor and co-workers,[22,23] the treatment of 1,10-phenanthroline monohydrochloride monohydrate with bromine in bromobenzene

(30) Croke, D. T.; Perrouault, L.; Sari, M. A.; Battioni, J. P.; Mansuy, D.; Helene, C.; Le Doan, J. *J. Photochem. Photobiol.* **1993**, *18*, 41–50.
(31) Praseuth, D.; Gaudemer, A.; Verlhac, J. B.; Kraljic, I.; Sissoeff, I.; Guille, E. *Photochem. Photobiol.* **1986**, *44*, 717–724.
(32) *Viability Staining Using Ethidium Bromide and Acridine Orange*; Technical Report, BD Biosciences: Mississauga, Ontario, Canada, **2008**.
(33) Parks, D. R.; Bryan, V. M.; Oi, V. M.; Oi, V. T.; Herzenberg, L. A. *Proc. Natl. Acad. Sci. U.S.A.* **1979**, *76*, 1962.

Chart 3. Synthesis of Diimine Ligands **2** and **3**

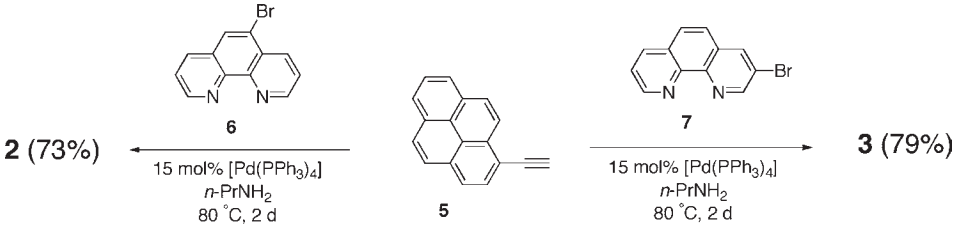

Table 1. Electronic Absorption and Emission Data for Ligands **2** and **3**, Their Ru(II) Complexes, and Model Compounds (10 μM MeCN)

compound	λ_{max} absorption (log ϵ), nm	λ_{em}, nm
2	235 (5.02), 282 (4.79), 315 (4.52), 376 (4.84), 397 (4.82)	449 (s)
3	236 (4.53), 285 (4.41), 312 (4.14), 376 (4.41), 398 (4.41)	458 (s)
1,10-Phenanthroline	230 (4.71), 264 (4.48), 280 (4.08)	
Pyrene	262 (4.31), 272 (4.61), 306 (3.98), 319 (4.38), 335 (4.59)	427 (s)
7	235 (4.91), 283 (5.03), 385 (4.59), 417 (4.65), 451 (4.48)	609 (vw)
8	237 (4.88), 282 (5.01), 385 (4.60), 417 (4.50), 474 (4.14)	625 (w)
$[Ru(bpy\text{-}d_8)_2(phen)]^{2+}$	263 (4.87), 285 (4.91), 448 (4.31)	615 (s)

for 36 h at 135 °C gave a 50% yield of a 1:1 mixture of 3-bromo-1,10-phenanthroline (**6**) and 3,8-dibromo-1,10-phenanthroline. Other brominated 1,10-phenanthrolines were formed in small amounts depending upon the temperature, concentration, and rate of addition. The desired **6** could be isolated in pure form by careful chromatography on alumina or selective acidification using HCl in ether. The subsequent reaction of **6** with **4** under the previously employed Sonogashira coupling conditions led to the formation of 3-(pyren-1′-yl)ethynyl-1,10-phenanthroline (**3**) in 79% yield (Chart 3).

The ligands **2** and **3** are unsymmetrical with respect to their diimine binding sites, and thus, the formation of their heteroleptic $[Ru(L)(bpy)_2]^{2+}$ complexes produces non-equivalence in all protons, leading to highly complex ^{1}H NMR spectra. To simplify the spectra, we prepared the corresponding perdeuterio bipyridine complexes,[34] having NMR-silent bipyridine protons. This isotopic labeling was accomplished by treating **2** or **3** with 1 equiv of $[Ru(bpy\text{-}d_8)_2Cl_2]$[35] in refluxing ethanol to afford the complexes in yields of 66−67%.

There are several notable features in the NMR spectra that allow for straightforward characterization. When H3 on 1,10-phenanthroline is replaced by an ethynylpyren-1-yl group, this proton resonance disappears as does the 3-bond coupling with H2 and H4, leaving these two protons as signals 9.45 and 8.54 ppm having a 1.8 Hz 4-bond coupling. With the disappearance of H3 at higher field, only H8 appears in this region (7.66 ppm) as a very characteristic doublet of doublets. Interestingly, H5 and H6 show magnetic equivalence and give rise to a singlet at 7.82 ppm. For the 5-substituted isomer, the pyridine ring protons H2, H3, H4 and H7, H8, H9 are non-equivalent, with the biggest difference being between H4 and H7 since the former is strongly deshielded (9.09 ppm) by the proximal ethynylpyrenyl group. H6 now appears as a singlet, also deshielded and shifted downfield. Upon complexation with $[Ru(bpy\text{-}d_8)_2]^{2+}$, the H2 and H9 resonances shift upfield because of shielding by one of the coordinated bipyridines. This shielding effect is less dramatic when H3 is replaced by ethynylpyrene. The H3 and H8 resonances at higher field are once again quite characteristic. For the complex of **2** there are two signals; one of these signals disappears in the complex of **3**.

The electronic absorption spectra of **2** and **3** were measured, and the data are recorded in Table 1. Compared to 1,10-phenanthroline (λ_{max} = 280 nm) and pyrene (λ_{max} = 335 nm), both measured in CH_3CN, the two ethynylpyrenyl derivatives show a substantial red-shift of their long wavelength $\pi\pi^*$ band. The substitution of a single ethynylpyrenyl group onto the 1,10-phenanthroline nucleus leads to a long wavelength absorption maximum at 397 nm (**2**) or 398 nm (**3**). It appears that 1,10-phenanthroline and pyrene subunits are effectively coupled electronically through the alkynyl linker, which explains the lower energy absorptions for the dyad systems as compared to the component chromophores.

The electronic absorption spectra of the $[Ru(bpy\text{-}d_8)_2(L)]^{2+}$ complexes where L = **2** or **3** were measured in acetonitrile, and the data are also recorded in Table 1. A long wavelength metal-to-ligand charge transfer (MLCT) absorption is observed in the region of 451−474 nm and can be compared with the corresponding absorption at 448 nm for the analogous complex where L = phen. The system having the ethynylpyrenyl substituent at the 5-position (λ_{max} = 451 nm) is the most similar to the parent 1,10-phenanthroline complex, indicating that charge delocalization through the 5-position is less effective than through the 3-position, where the MLCT absorption is found at 474 nm. Although the ligands show strong pyrene-based emission at 449−458 nm, the corresponding Ru(II) complexes are nearly non-emissive at room temperature. Excitation spectra indicate that trace $[Ru(bpy)_3]^{2+}$ is not responsible for this weak emission.

The half-wave redox potentials of the complexes were measured by cyclic voltammetry, and the results are summarized in Table 2. The first oxidation wave of Ru(II) polypyridyl complexes is generally associated with the removal of an electron from a metal-based d orbital and,

(34) In our experience perdeuteration of the ancilliary ligands of the Ru(II) complexes does not significantly alter their DNA photocleaving properties or photophysics.

(35) Chirayil, S.; Thummel, R. P. *Inorg. Chem.* **1989**, *28*, 812–813.

Table 2. Cyclic Voltammetric Data for 1,10-Phenanthroline and Ru(II) Complexes **7** and **8**[a]

compound	$E^{red}_{1/2}$ (ΔE)		$E^{red}_{1/2}$ (ΔE)	
[Ru(phen)-(bpy)$_2$](PF$_6$)$_2$	+1.27 (74)	−1.36 (77)	−1.55 (84)	−1.79 (86)
7	+1.32 (128)	−1.11^{ir}	−1.48 (98)	−1.81^{ir}
8	+1.31 (107)	−1.21 (79)	−1.45 (107)	−1.81^{ir}

[a] Spectra were recorded in MeCN containing 0.1 M NBu_4PF_6 at a scan rate of 100 mV/s. $E_{1/2}$ is reported as V vs SCE, and ΔE as mV. The notation *ir* represents an irreversible process, and the value was estimated by differential peaks.

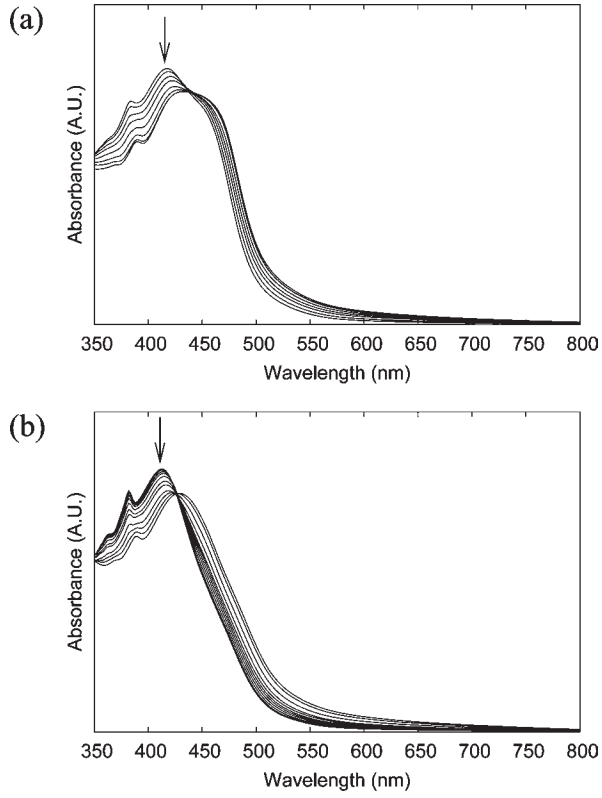

Figure 1. Titrations of 10 μM solutions of **7** (a) and **8** (b) with herring sperm DNA (10 mM MOPS, pH 7.5).

in this regard, is less influenced by subtle changes in the identity of the ligands. The observed potentials of +1.31 and +1.32 V are close to the potential of +1.27 measured for the parent $[Ru(bpy)_2(phen)]^{2+}$ complex. The reductions are ligand-based, and the first reduction potentials of −1.11 and −1.21 V observed for complexes **7** and **8** are slightly more positive than the parent complex (−1.36 V), which is consistent with the increased delocalization expected for these more conjugated systems. The second and third reductions probably take place on the auxiliary bpy ligands and, thus, these potentials fall within 0.10 V for all three systems.

3.2. DNA Binding. To discern possible interactions with DNA, 10 μM solutions of **7** and **8** were titrated with DNA in a variety of buffered solutions at pH 7.5. The spectral responses of both **7** and **8** to added DNA were highly dependent on the source of DNA used as titrant (calf thymus vs herring sperm DNA), the buffering system (MOPS vs Tris-HCl), and the ionic strength of

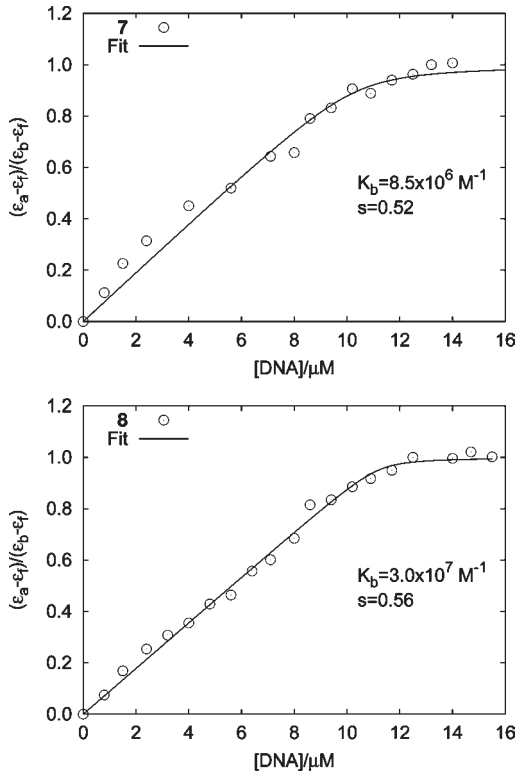

Figure 2. Binding isotherms for **7** (414 nm) and **8** (412 nm) with herring sperm DNA (10 mM MOPS, pH 7.5).

the solution (0 vs 50 mM NaCl). Generally, the ligand-centered $\pi\pi^*$ and MLCT absorption transitions associated with the dyads shifted to longer wavelengths (bathochromism) and were reduced in intensity (hypochromism) with increasing concentration of DNA regardless of the conditions employed. The largest red-shifts (16−18 nm) for both **7** and **8** were observed with calf thymus DNA as titrant in 10 mM MOPS (pH 7.5) and were accompanied by 15% and 20% absorbance attenuations, respectively. As expected, these hypochromicities were slightly reduced when the ionic strength of the solution was increased by addition of 50 mM NaCl and were enhanced when measured at the blue-edge of the visible MLCT transitions or when the source of DNA was herring sperm. Figure 1 illustrates optical titrations of **7** and **8** with herring sperm DNA (10 mM MOPS, pH 7.5) over a narrow concentration range ([DNA]/[Ru] = 0.1−2), where clear isosbestic points are evident.[36] DNA binding constants (K_b) for **7** and **8** were calculated to be $8.5 \times 10^6\ M^{-1}$ and $3.0 \times 10^7\ M^{-1}$, respectively, from fits of the absorption changes as a function of DNA concentration to eq 1 (Figure 2). Both the spectral responses and the magnitudes of K_b for the dyads are similar to what have been observed for known Rh(III) and Ru(II) metallointercalators ($K_b > 10^6\ M^{-1}$) containing the dppz ligand.[4,5,7,37] While base pair binding bite

(36) In many of the buffering systems employed, no clear isosbestic points could be discerned. However, provided that ratios of [DNA] to [Ru] were chosen to minimize aggregation of the dyads under low-salt conditions, similar binding constants were obtained from the absorbance hypochromicities.

(37) Friedman, A. E.; Chambron, J. C.; Sauvage, J. P.; Turro, N. J.; Barton, J. K. *J. Am. Chem. Soc.* **1990**, *112*, 4960–4962.

sizes for metallointercalators are generally greater than 1,[29,38−40] *s* values for the dyads are 0.52 and 0.56, respectively. Base pair binding site sizes less than unity, as calculated for **7** and **8**, have been interpreted by others to mean that intercalator molecules are stacking with each other on the DNA surface.[41,42]

Given that polycyclic aromatic hydrocarbons intercalate into DNA,[43−50] albeit more weakly than cationic intercalators such as ethidium bromide ($K_b = 1.7 \times 10^5\ M^{-1}$),[51,52] it is reasonable to conclude that the ethynylpyrenyl units in dyads **7** and **8** provide a handle for intercalation between DNA base pairs and that this interaction is enhanced by the cationic metal center. In this scenario DNA binding appears to be somewhat stronger with 3-substitution of the ethynylpyrenyl group on the 1,10-phenanthroline ring. However, caution must be used in assigning intercalation as the preferred DNA binding mode from only optical titration data since DNA intercalation, groove binding, and external association can all induce qualitatively similar effects via spectroscopic methods.[53] Spectral hypochromicity and bathochromicity, which generally arise from π-stacking interactions that are favored in polar media,[54−57] have been observed for some minor groove binders such as 4′,6-diamidino-2-phenylindole (DAPI).[58] Additionally, it is well-documented that polyanions like DNA facilitate the aggregation of hydrophobic molecules at their surfaces in aqueous solutions.[59] Therefore, DNA thermal denaturation measurements[60−63] and relative viscosity changes[64] of DNA solutions served as additional probes for DNA intercalation as an important binding mode for the dyads.

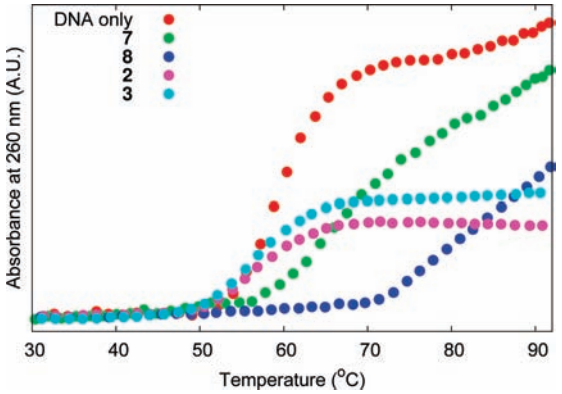

Figure 3. Thermal denaturation of calf-thymus DNA (24 μM base pairs, 10 mM MOPS, pH 7.4) alone and in the presence of ligands (**2**, **3**) or dyads (**7**, **8**).

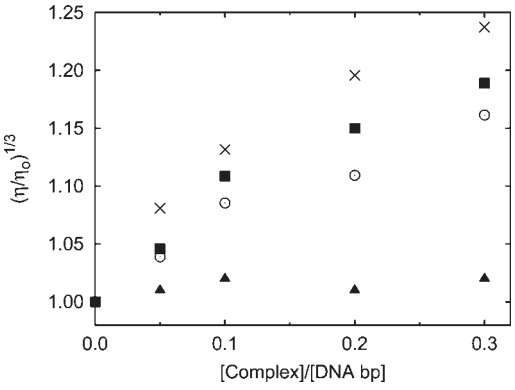

Figure 4. Relative viscosity changes of calf thymus DNA solutions with increasing concentrations of **7** (⊙) and 8 (×). Ethidium bromide (■) and Hoechst 33258 (▲) are included for comparison.

The melting temperature (T_m) of calf thymus DNA in 10 mM MOPS (pH 7.4) was determined to be 60 ± 2 °C, and changes in T_m induced by the dyads are shown in Figure 3. The presence of ligand **2** or **3** (5 μM) as the free base, lacking the favorable electrostatic component for DNA interaction, did not significantly alter the melting temperature of DNA,[65] underscoring the importance of the cationic metal center for DNA binding. Addition of **7** or **8** (5 μM) increased T_m by 10 and 20 °C, respectively. The large increase in T_m for **8**, $\Delta T_m >$ 20 °C, is consistent with ΔT_m values reported for known intercalators such as $[Rh(phi)_2(phen)]^{3+}$ (phi = 9,10-phenanthrenequinone diimine).[66] The attenuated ΔT_m measured for **7**, while still suggestive of intercalation or partial intercalation, illustrates that positioning of the ethynylpyrenyl group relative to the 1,10-phenanthroline ring can be used to influence the magnitude of this DNA interaction.

Hydrodynamic methods provided further support for DNA intercalation by both **7** and **8**. Figure 4 shows an

(38) Welch, T. W.; Corbett, A. H.; Thorp, H. H. *J. Phys. Chem.* **1995**, *99*, 11757–11763.
(39) Johnston, D. H.; Thorp, H. H. *J. Phys. Chem.* **1996**, *100*, 13837–13843.
(40) Neyhart, G. A.; Grover, N.; Smith, S. R.; Kalsbeck, W. A.; Fairley, T. A.; Cory, M.; Thorp, H. H. *J. Am. Chem. Soc.* **1993**, *115*, 4423–4428.
(41) Nair, R. B.; Teng, E. S.; Kirkland, S. L.; Murphy, C. J. *Inorg. Chem.* **1998**, *37*, 139–141.
(42) Haq, I.; Lincoln, P.; Suh, D.; Norden, B.; Chowdhry, B. Z.; Chaires, J. B. *J. Am. Chem. Soc.* **1995**, *117*, 4788–4796.
(43) Wolfe, A.; Shimer, G. H., Jr.; Meehan, T. *Biochemistry* **1987**, *26*, 6392–6396.
(44) Berman, H. M.; Young, P. R. *Annu. Rev. Biophys. Bioeng.* **1981**, *10*, 87–114.
(45) Dougherty, G.; Pilbrow, J. R. *Int. J. Biochem.* **1984**, *16*, 1179–1192.
(46) Geacintov, N. E.; Prusik, T.; Khosrofian, J. M. *J. Am. Chem. Soc.* **1976**, *98*, 6444–6452.
(47) Geacintov, N. E.; Gagliano, A.; Ivanovic, V.; Weinstein, I. B. *Biochemistry* **1978**, *17*, 5256–5262.
(48) Ibanez, V.; Geacintov, N. E.; Gagliano, A. G.; Brandimarte, S.; Harvey, R. G. *J. Am. Chem. Soc.* **1980**, *102*, 5661–5666.
(49) Meehan, T.; Gamper, H.; Becker, J. F. *J. Biol. Chem.* **1982**, *257*, 10479–10485.
(50) Nagata, C.; Kodama, M.; Tagashira, Y.; Imamura, A. *Biopolymers* **1966**, *4*, 409–427.
(51) Tang, T. C.; Huang, H. J. *Electroanalysis* **1999**, *11*, 1185–1190.
(52) Paoletti, C.; Le Pecq, J. B.; Lehman, I. R. *J. Mol. Biol.* **1971**, *55*, 75–100.
(53) Li, H. J.; Crothers, D. M. *J. Mol. Biol.* **1969**, *39*, 461–477.
(54) Felthouse, T. R. *Prog. Inorg. Chem.* **1982**, *29*, 73–166.
(55) Bilakhiya, A. K.; Tyagi, B.; Paul, P.; Natarajan, P. *Inorg. Chem.* **2002**, *41*, 3830–3842.
(56) Jones, G.; Vullev, V. I. *J. Phys. Chem. A* **2001**, *105*, 6402–6406.
(57) Jockusch, S.; Turro, N. J.; Tomalia, D. A. *Macromolecules* **1995**, *28*, 7416–7418.
(58) Kubista, M.; Åkerman, B.; Nordén, B. *Biochemistry* **1987**, *26*, 4545–4553.
(59) Wang, M.; Silva, G. L.; Armitage, B. A. *J. Am. Chem. Soc.* **2000**, *122*, 9977–9986.
(60) Sinan, M.; Panda, M.; Ghosh, A.; Dhara, K.; Fanwick, P. E.; Chattopadhyay, D. J.; Goswami, S. *J. Am. Chem. Soc.* **2008**, *130*, 5185–5193.
(61) Kumar, C. V.; Asuncion, E. H. *J. Am. Chem. Soc.* **1993**, *115*, 8547–8553.
(62) Patel, D. J. *Acc. Chem. Res.* **1979**, *12*, 118–125.
(63) Patel, D. J.; Canuel, L. L. *Proc. Natl. Acad. Sci. U.S.A.* **1976**, *73*, 3343–3347.
(64) Suh, D.; Oh, Y.; Chaires, J. B. *Process Biochem.* **2001**, *37*, 521–525.
(65) The absorbance signal at 260 nm contains contributions from both DNA and the potential DNA binder. Therefore, the maximum signal obtainable is attenuated for ligands 2 and 3 owing to their reduced extinction coefficients at this wavelength relative to the dyads.
(66) Fu, P.; Bradley, P. M.; Turro, C. *Inorg. Chem.* **2003**, *42*, 878–884.

increase in the relative viscosities of DNA solutions containing these complexes. Intercalators unwind the double helix by a defined angle when they insert between base pairs, producing DNA that is somewhat elongated relative to canonical B-form DNA. Lengthening of the helical axis gives rise to measurable increases in viscosity[64] that are not observed for other common types of DNA binding, namely, groove-binding or electrostatic association, or DNA-templated aggregation of hydrophobic chromophores. When 150 μM DNA (base pairs) was treated with increasing concentrations of **7** or **8**, the relative viscosity increased substantially. In fact, **8** produced a larger change in viscosity than the known intercalator ethidium bromide. Consistent with thermal denaturation experiments, **7** produced a smaller increase in solution viscosity but still notably greater than the minor-groove binder Hoechst 33258, which is included for comparison.

Together the optical titrations, thermal denaturation studies, and relative viscosity measurements point toward intercalation as one important mode of binding to DNA by this class of molecules. The ethynylpyrenyl handle is likely the point of attachment to DNA as planar, aromatic systems are known to intercalate through efficient π-stacking between the DNA base pairs. It is interesting to note that ligands **2** and **3** (as their free bases) did not interact substantially with DNA. Tethering these organic chromophores in a Ru(II) diimine dyad such as **8** appears to be a prerequisite for strong DNA binding and reinforces the association with DNA over known cationic intercalators such as ethidium bromide. The attenuated binding of **7** relative to **8** reveals that the magnitude of the DNA-binding interaction is sensitive to the substitution pattern on the 1,10-phenanthroline functionality and may, in turn, influence the extent of photoreactivity toward DNA (vide supra).

3.3. DNA Photocleavage. As shown in Figure 5, both **7** and **8** cause extensive damage to DNA when irradiated with visible light. Plasmid DNA served as a convenient probe for DNA photocleavage, whereby gel electrophoretic analysis with ethidium-bromide staining was used to distinguish three distinct topological forms of DNA: Form I (supercoiled), Form II (relaxed), and Form III (linear). The topological state of plasmid DNA, in turn, reflects the nature of DNA damage mediated by a photoactivatable agent: single- or double-strand breaks in the backbone as well as unwinding of the double helix. Form I DNA (Figure 5a, lane 1), often referred to as closed, circular DNA, represents native plasmid DNA that is negatively supercoiled in the absence of DNA damaging agents. When single-strand breaks occur, superhelical tension is removed and the DNA relaxes to produce Form II (Figure 5a, lane 12), which migrates more slowly through the agarose gel as nicked, circular DNA. If two single-strand lesions occur within approximately 15 base pairs[67] or if frank double-strand cleavage takes place, the result is linear, Form III DNA (Figure 5c, lane 13), which travels between Forms I and II on the gel. DNA photocleavage assays with pUC19 or pBR322 plasmid and complex **7** or **8** showed no DNA damage in the dark (Figure 5a, lane 13 and Figure 5b, lane 13). Similarly, irradiation of the plasmids alone for 30 min

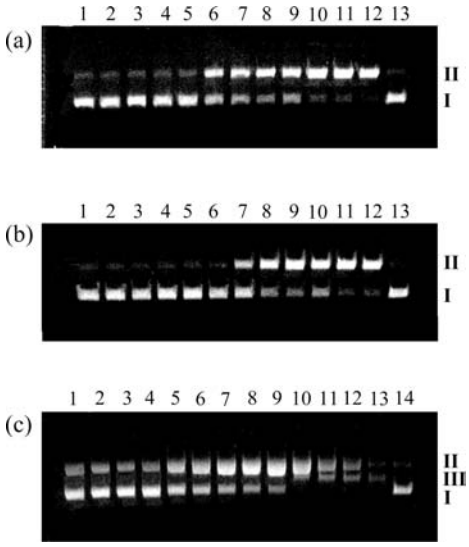

Figure 5. Gel electrophoretic analysis of DNA photocleavage titrations in air (1% agarose gel containing 0.75 μg mL^{-1} ethidium bromide, 1X TAE, 8 V cm^{-1}, 30 min.). (a) and (b) contain pUC19 plasmid; (c) contains p*Des*R3 plasmid. (a) Lane 1, plasmid only; lane 2, 50 nM **7**; lane 3, 100 nM **7**; lane 4, 250 nM **7**; lane 5, 500 nM **7**; lane 6, 750 nM **7**; lane 7, 1.00 μM **7**; lane 8, 1.25 μM **7**; lane 9, 1.50 μM **7**; lane 10, 1.75 μM **7**; lane 11, 2.00 μM **7**; lane 12, 2.25 μM **7**; lane 13, 2.25 μM **7** ($-h\nu$). (b) Lane 1, plasmid only; lane 2, 25 nM **8**; lane 3, 50 nM **8**; lane 4, 75 nM **8**; lane 5, 100 nM **8**; lane 6, 300 nM **8**; lane 7, 500 nM **8**; lane 8, 750 nM **8**; lane 9, 1.00 μM **8**; lane 10, 1.25 μM **8**; lane 11, 1.50 μM **8**; lane 12, 2.00 μM **8**; lane 13, 2.00 μM **8** ($-h\nu$). (c) Lane 1, plasmid only; lane 2, 25 nM **8**; lane 3, 50 nM **8**; lane 4, 100 nM **8**; lane 5, 500 nM **8**; lane 6, 750 nM **8**; lane 7, 1.00 μM **8**; lane 8, 1.50 μM **8**; lane 9, 2.00 μM **8**; lane 10, 3.00 μM **8**; lane 11, 5.00 μM **8**; lane 12, 7.00 μM **8**; lane 13, 10.0 μM **8**; lane 14, 10.0 μM **8** ($-h\nu$).

with 420 nm light (typical light-assay conditions) resulted in no discernible DNA damage. However, irradiation of either **7** or **8** in the presence of pUC19 or pBR322 plasmid produced single-strand breaks in a concentration-dependent manner, with EC_{50} (effective concentration) values in the nanomolar regime and complete single-strand cleavage (100% Form II) occurring at concentrations of complex near 2 μM. Notably, when the GC content of the plasmid was increased (e.g., pDesR3), **8** elicited double-strand breaks at concentrations above 3 μM (Figure 5c). The appearance of Form III DNA on the gel was only apparent at concentrations above that which caused complete single-strand scission, suggesting that double-strand cleavage may arise from the accumulation of single-strand breaks that occur within a critical distance on the helix.[68,69] Unfortunately, the gradual disappearance of both Form II and Form III bands at higher concentrations of **8** precluded a detailed analysis of this behavior since the ethidium bromide intercalating dye was not able to penetrate the helix at elevated concentrations of **8**. Surprisingly, **7** did not linearize plasmid DNA under similar conditions despite having a larger extinction coefficient at the irradiating wavelength, underscoring the importance of the 3-substitution pattern for the more deleterious double-strand DNA cleavage. Enhanced differences in DNA-binding affinity (vide infra) or photoreactivity toward DNA with higher %GC may reflect some sequence selectivity for the dyads, especially **8**.

(67) Freifelder, D.; Trumbo, B. *Biopolymers* **1969**, *7*, 681–693.

(68) OhUigin, C. Ph.D. thesis, University of Dublin, **1988**.

(69) Åkerman, B.; Tuite, E. *Nucleic Acids Res.* **1996**, *24*, 1080–1090.

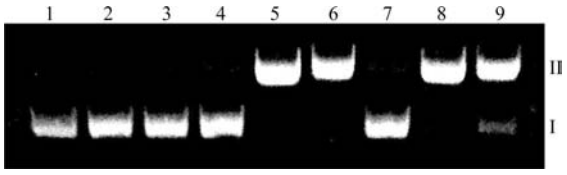

Figure 6. Comparison of DNA photocleavage by **7** and **8** for air-saturated and deoxygenated solutions by gel electrophoretic analysis (1% agarose gel containing 0.75 μg mL^{-1} ethidium bromide, 1X TAE, 8 V cm^{-1}, 30 min.). Lanes 1−4 and 7 are control lanes, and lanes 5−6 and 8−9 are reaction lanes: lane 1, pUC19 plasmid only (−*hv*); lane 2, pUC19 plasmid in air-saturated solution; lane 3, pUC19 plasmid in argon-purged solution; lane 4, pUC19 plasmid incubated for 30 min at 37 °C in air-saturated solution containing 2 μM **7** (−*hv*); lane 5, pUC19 plasmid in air-saturated solution containing 2 μM **7**; lane 6, pUC19 in argon-purged solution containing 2 μM **7**; lane 7, pUC19 plasmid incubated for 30 min at 37 °C in air-saturated solution containing 2 μM **8** (−*hv*); lane 8, pUC19 plasmid in air-saturated solution containing 2 μM **8**; lane 9, pUC19 in argon-purged solution containing 2 μM **8**.

Despite their abilities to photosensitize $^1O_2$ in the absence of DNA,[70] **7** and **8** showed little attenuation in DNA photocleavage in the absence of oxygen, in the presence of reactive oxygen scavengers, or in D_2O buffer. This oxygen-independence is quite notable in that mononuclear polypyridyl Ru(II) complexes typically rely on singlet-oxygen generation for DNA photocleavage,[71−75] and the ensuing DNA damage is much less efficient. Figure 6 (Lanes 2−3) indicates that irradiation of plasmid DNA with visible light for 30 min under ambient or deoxygenated conditions results in no detectable strand breaks in the DNA backbone. Similarly, incubation of 2 μM **7** (Lane 4) or **8** (Lane 7) with plasmid DNA in the dark (10 mM MOPS, pH 7.5, 0.1 mM NaCl) produces no discernible DNA damage. Lanes 5 and 6 clearly show that there is no difference in the extent of single-strand photocleavage by **7** when oxygen is removed, and only a slight inhibition of strand breakage occurs for deoxygenated samples of **8** (Lanes 8−9). While some Rh(III) complexes are known to photocleave DNA via both oxygen-dependent and oxygen-independent pathways,[7,76] few Ru(II) complexes have been shown to operate under hypoxic conditions, and these utilize at least two metals working in concert and, in some cases, require the presence of glutathione.[77−79] Thus, the discovery of a relatively simple mononuclear Ru(II) motif that leads to efficient DNA photocleavage under hypoxic conditions is particularly intriguing for phototherapeutic applications such as PDT, whereby the search for new drugs that target hypoxic tumors remains a significant challenge. It is often these oxygen-deprived tumor cells that are the most resistant to radiotherapy[80,81] and chemotherapy[82,83] and particularly susceptible to metastasis.[84,85]

The observation that both **7** and **8** photocleave DNA in the absence of oxygen without the use of a sacrificial electron acceptor implies that reactive excited states, other than the commonly employed ^{3}MLCT state for $^1O_2$ sensitization, may be involved. In fact, dirhodium complexes of dppz, which exhibit some oxygen-independence, are thought to react with DNA through a low-lying triplet state that may be associated more with the π-extended ligand, creating a long-lived, charge-separated state that results in oxidative DNA photocleavage by the dirhodium core.[7] Unusually long excited-state lifetimes ($\tau \sim 42$ μs) have been measured for pyrene-Ru(II) polypyridine dyads derived from the bipyridyl counterpart of ligand **3** and are thought to arise from intramolecular triplet energy transfer involving the lowest-lying ^{3}MLCT state and a ligand-centered $^3\pi\pi^*$ state.[18] A similar equilibrium may be at play in the pyrene-Ru(II) 1,10-phenanthroline dyads, allowing the quasi-oxidized Ru^{3+} center to react directly with DNA through guanine oxidation. The enhanced photocleavage observed for DNA with higher %GC supports this proposed mechanism, and a detailed investigation to elucidate the photophysics of the ethynylpyrenyl-1,10-phenanthroline Ru(II) dyads and the nature of the reactive excited states that photocleave DNA is underway.

3.4. Cytotoxicity and Photocytotoxicity. The cytotoxicity and photocytotoxicity of **7** and **8** toward human leukemia cells (HL-60) in culture was determined by measuring percent viability as a function of increasing concentrations of the dyads with and without irradiation with visible light. These measurements were made relative to growing cultures that were not subjected to potentially cytotoxic agents or light. Interpolation of the collected data was used to highlight the concentration of dyad necessary to achieve a 50% loss in viability, which is designated LC_{50} (LC = lethal concentration). As shown in Figure 7a, the LC_{50} for **7** in the dark is approximately 15 μM. In the absence of **7**, there is only a marginal loss in viability (< 10%) caused by irradiation of the cells, and, in most instances, there was no detectable loss in viability under the irradiation conditions employed. When growing cultures containing **7** were irradiated for 30 min with visible light, the LC_{50} decreased to well below 5 μM. Notably, at concentrations between 5 and 10 μM **7**, there is a 50% loss in the viability of the irradiated cells over the control cells that were incubated with **7** in the dark. This enhanced photocytotoxicity relative to the dark controls is an essential property for a photochemotherapeutic agent and is exemplified in the case of **8**. Figure 7b demonstrates that there is <5% loss in the viability of

(70) Emission from singlet oxygen at 1268 nm was observed for solutions of 7 and 8 upon photoirradiation in acetonitrile or 4:1 EtOH/MeOH. Quantum yields for singlet oxygen generation were not measured.
(71) Liu, Y.; Hammitt, R.; Lutterman, D. A.; Joyce, L. E.; Thummel, R. P. *Inorg. Chem.* **2009**, *48*, 375–385.
(72) Chouai, A.; Wicke, S. E.; Turro, C.; Bacsa, J.; Dunbar, K. R.; Wang, D.; Thummel, R. P. *Inorg. Chem.* **2005**, *44*, 5996–6003.
(73) Clarke, M. J. *Coord. Chem. Rev.* **2003**, *236*, 209–233.
(74) Hergueta-Bravo, A.; Jimenez-Hernandez, M. E.; Montero, F.; Oliveros, E.; Orellana, G. *J. Phys. Chem. B* **2002**, *106*, 4010–4017.
(75) Fu, P. K.-L.; Bradley, P. M.; van Loyen, D.; Dürr, H.; Bossman, S. H.; Turro, C. *Inorg. Chem.* **2002**, *41*, 3808–3810.
(76) Bradley, P. M.; Angeles-Boza, A. M.; Dunbar, K. R.; Turro, C. *Inorg. Chem.* **2004**, *43*, 2450–2452.
(77) Swavey, S.; Brewer, K. J. *Inorg. Chem.* **2002**, *41*, 6196–6198.
(78) Holder, A. A.; Swavey, S.; Brewer, K. J. *Inorg. Chem.* **2004**, *43*, 303–308.
(79) Janaratne, T. K.; Yadav, A.; Ongeri, F.; MacDonnell, F. M. *Inorg. Chem.* **2007**, *46*, 3420–3422.
(80) Gatenby, R. A.; Kessler, H. B.; Rosenblum, J. S.; Coia, L. R.; Moldofsky, P. J.; Hartz, W. H.; Broder, G. J. *Int. J. Radiat. Oncol. Biol. Phys.* **1988**, *14*, 831–838.
(81) Hockel, M.; Knoop, C.; Schlenger, K.; Vorndran, B.; Baubmann, E.; Mitze, M.; Knapstein, P. G.; Vaupel, P. *Radiother. Oncol.* **1993**, *26*, 45–50.
(82) Sartorelli, A. C. *Cancer Res.* **1988**, *48*, 775–778.
(83) Tannock, I.; Guttman, P. *Br. J. Cancer* **1981**, *42*, 245–248.
(84) Sundfor, K.; Lyng, H.; Rofstad, E. K. *Br. J. Cancer* **1998**, *78*, 822–827.
(85) Rofstad, E. K.; Danielson, T. *Br. J. Cancer* **1999**, *80*, 1697–1707.

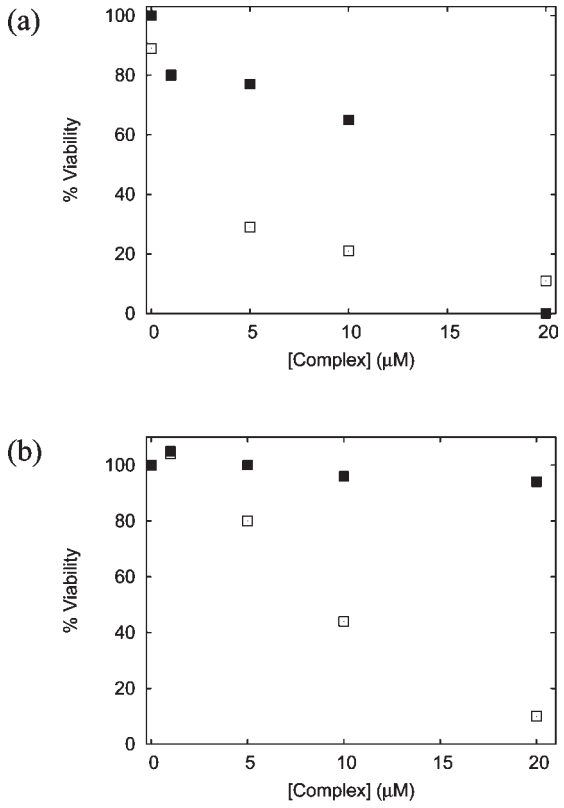

Figure 7. Plots of percent viability of human promyelocytic leukemia cells (HL-60) as a function of concentration of (a) **7** and (b) **8** in the dark (■) and irradiated with visible light for 30 min (⊡).

the cells when incubated with **8** in the dark over the concentration range investigated, precluding an estimation of the LC_{50}. Remarkably, the viability of irradiated cultures containing 10 μM **8** was reduced by 60%, and 20 μM **8** resulted in ~90% increase in toxicity relative to the dark controls.

Results obtained from nuclear morphology staining with the AO-EB dye combination[32,33] correlated well with manual photo- and dark cytotoxicity determinations. Figures 8 and 9 illustrate the enhanced cytotoxicity observed when **7** and **8** are activated by visible light, respectively. Briefly, small aliquots were removed from the photo- and dark cytotoxicity assays (used for the manual cell counts) and stained with a mixture of AO-EB in PBS. In these experiments a microscope operating in epi-fluorescence mode was used to illuminate the stained cells and capture the resulting fluorescence from the dyes. It is well-established that AO is able to penetrate the membranes of viable cells while EB is excluded. Therefore, green fluorescence from AO is a convenient marker for viable cells, and red fluorescence from EB indicates a loss of cell viability. At the concentrations shown, there is no significant loss in cell viability for HL-60 cells exposed to **7** or **8** in the dark, and, thus, they fluoresce green as expected. However, increasing concentrations of **7** or **8**, respectively, result in larger fractions of cells that fluoresce red. These nonviable cells, having compromised membranes, may be apoptotic or necrotic, which can be discerned by viewing with increased magnification. Figure 10 (left panel) illustrates the photocytotoxicity produced by **7** and **8** when viewed with the same magnification as shown in Figures 8 and 9; increasing the magnification by 4-fold or 10-fold (b and e, respectively) reveals the formation of apoptotic bodies quite clearly. These apoptotic bodies (zoomed for clarity in the right panel) are formed from surface blebbing of the membrane that occurs subsequent to DNA condensation and fragmentation in response to programmed cell death. Photocytotoxicity resulting from the induction of apoptosis in HL-60 cells that were exposed to the dyads and irradiated is a remarkable finding. For photobiology applications such as PDT, apoptosis is the preferred mode of cell death as necrosis is a rather traumatic form of cellular destruction that is accompanied by intense inflammation of surrounding tissue and the rupturing of extended blood vessels in vivo.[86,87] Because the latter often hinders further PDT treatment, much effort to improve PDT agents is aimed at controlling the outcome of photosensitization by careful minimization of tissue necrosis.

The lack of significant cytotoxic activity in the dark at relatively low concentrations of **7** and **8** is somewhat surprising given the ability of the dyads to intercalate DNA. Often, the topological changes to DNA that accompany intercalation disrupt crucial protein-nucleic acid interactions that control cellular function such as DNA replication and transcription. The result is a dark toxicity that usually parallels the strength of DNA binding. Interestingly, **8** interacts with DNA more strongly than **7** according to optical titrations, thermal denaturation studies, and relative viscosity changes, yet **7** is notably more cytotoxic than **8** toward HL-60 cells. Since **8** showed stronger DNA interactions and caused more deleterious DNA damage (i.e., double-strand scission of some plasmids) in non-cell-based assays, factors other than DNA-binding strength and reactivity must contribute to the differences in dark cytotoxicity documented for these dyads. It is well-known that cellular uptake of Ru(II) complexes is strongly influenced by the identity of the coordinating ligands, which control the overall complex charge, size, shape, and hydrophobicity.[88,89] Therefore, the nature of both the DNA-interacting and the ancillary ligands may have implications in the relative cytotoxicities of these systems. Regardless of the underlying mechanism responsible for the cytotoxicity and photocytotoxicity associated with **7** and **8**, it is evident from these studies that the position occupied by the ethynylpyrenyl substituent on the 1,10-phenanthroline ring has a considerable influence. Efforts are underway to determine the source of cytotoxicity and photocytotoxicity for the dyads and the role that positional isomerism plays in their corresponding mechanisms of action.

4. Concluding Remarks

Two new mononuclear Ru(II) complexes possessing the phenanthroline-appended ethynylpyrenyl ligands **2** and **3** were synthesized, characterized, and evaluated for their potential in photobiological applications such as PDT. Numerous techniques support intercalation as an important binding mode for dyads **7** and **8**, and both complexes

(86) Li, C. Z.; Cheng, L. F.; Wang, Z. Q.; Gu, Y. *Endoscopy* **2003**, *35*, 1043–1048.
(87) Ali, S. M.; Olivo, M. *Int. J. Oncol.* **2003**, *22*, 1181–1191.
(88) Puckett, C. A.; Barton, J. K. *Biochemistry* **2008**, *47*, 11711–11716.
(89) Puckett, C. A.; Barton, J. K. *J. Am. Chem. Soc.* **2007**, *129*, 46–47.

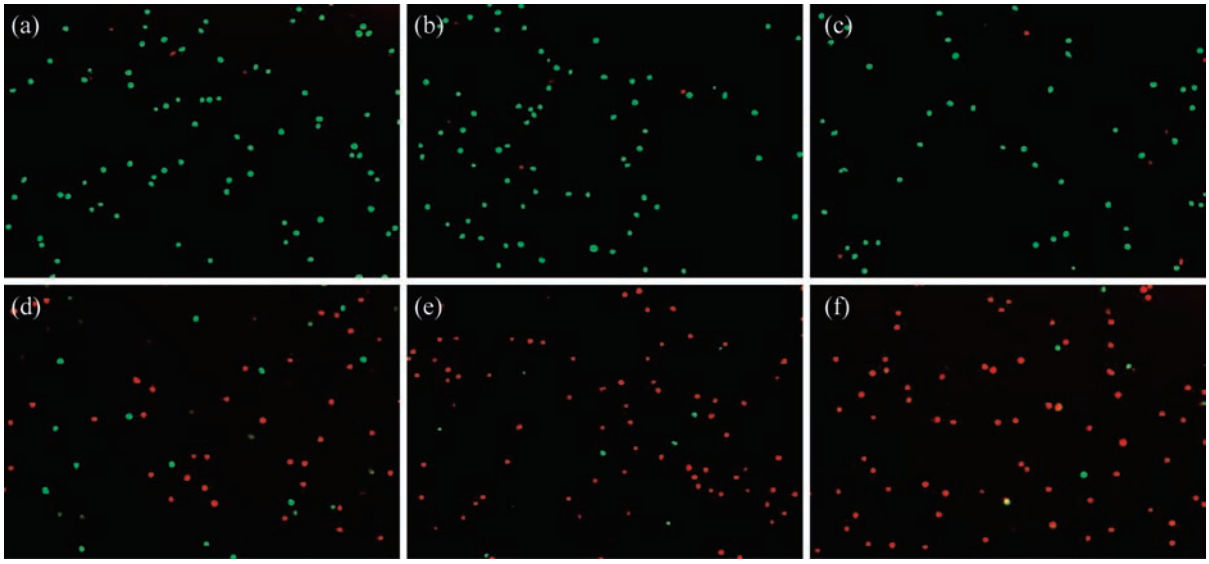

Figure 8. Cytotoxicity and photocytotoxicity of HL-60 cells with varying concentrations of **7** observed by nuclear morphology staining with AO-EB. (a) 1 μM **7**, $-hv$; (b) 5 μM **7**, $-hv$; (c) 10 μM **7**, $-hv$; (d) 1 μM **7**, $+hv$; (e) 5 μM **7**, $+hv$; (f) 10 μM **7**, $+hv$.

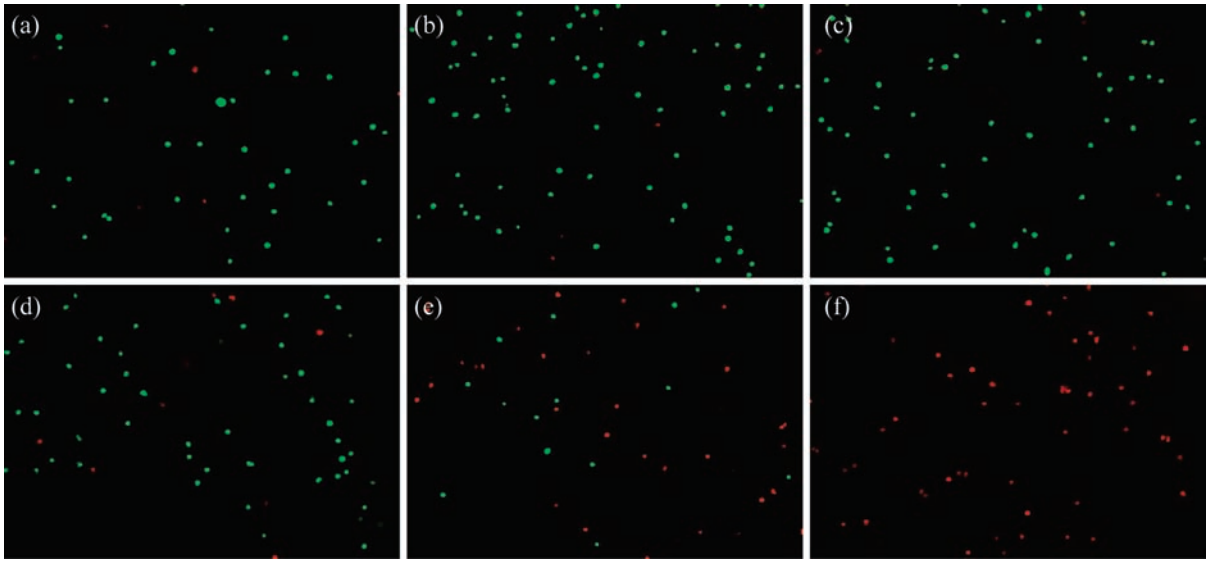

Figure 9. Cytotoxicity and photocytotoxicity of HL-60 cells with varying concentrations of **8** observed by nuclear morphology staining with AO-EB. (a) 5 μM **8**, $-hv$; (b) 10 μM **8**, $-hv$; (c) 20 μM **8**, $-hv$; (d) 5 μM **8**, $+hv$; (e) 10 μM **8**, $+hv$; (f) 20 μM **8**, $+hv$.

photocleave DNA in vitro when irradiated with visible light ($\lambda_{irr} \geq 400$ nm) at concentrations similar to those documented in DNA photocleavage assays for lutetium(III) texaphyrin (LuTx),[90,91] a photosensitizer currently used in PDT. DNA-binding and ensuing photocleavage are sensitive to the position of the ethynylpyrenyl substituent on the 1,10-phenanthroline ring, with **8** showing the strongest binding under all conditions and causing more deleterious damage to DNA. It is not clear whether the increased photoreactivity of **8** is correlated directly to a higher affinity for DNA, but a thorough photophysical investigation of the interactions of the dyads with DNA is currently underway and should help clarify this issue. Interestingly, these mononuclear Ru(II) dyads photocleave DNA under hypoxic conditions, an important step toward the design of new phototherapeutic agents since few systems demonstrate such activity in the absence of oxygen. The photoactivity of **7** and **8** translates well to cytotoxicity and photocytotoxicity models using human leukemia cells, where **7** and **8** show minimal or essentially no cytotoxicity in the dark at concentrations of 5−10 μM and 10−20 μM, respectively, and much higher toxicity when irradiated. Because the dark cytotoxicity associated with these dyads does not necessarily parallel DNA-binding strength or the magnitude of the DNA damage apparent in photocleavage assays, differences in cytotoxic activity may be influenced by differences in membrane penetration, subcellular localization, biological targets, or mechanisms of action. Consequently, this work provides evidence that agents incorporating strong-intercalating units do not a priori produce dark toxicity, discounting the popular tenet that DNA intercalation may not be a desirable property

(90) Allison, R. R.; Downie, G. H.; Cuenca, R.; Hu, X.-H.; Childs, C. J. H.; Sibata, C. H. *Photodiagn. Photodyn. Ther.* **2004**, *1*, 27–42.
(91) Magda, D.; Wright, M.; Miller, R. A.; Sessler, J.; Sansom, P. I. *J. Am. Chem. Soc.* **1995**, *117*, 3629–3630.

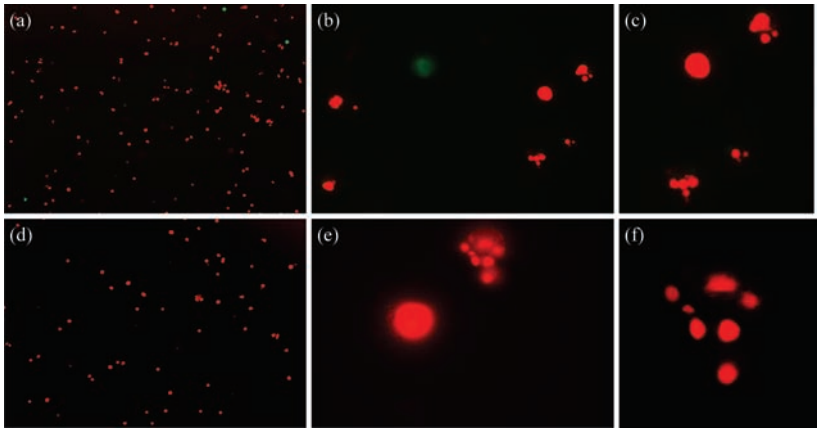

Figure 10. Formation of apoptotic bodies in HL-60 cells with **7** [(a)−(c)] and **8** [(d)−(e)] observed by nuclear morphology staining with AO-EB. (a) 10 μM **7**, + *hv*, 10X obj.; (b) 10 μM **7**, + *hv*, 40X obj.; (c) 10 μM **7**, + *hv*, 40X obj. (zoomed); (d) 20 μM **8**, + *hv*, 10X obj.; (e) 20 μM **8**, + *hv*, 100X obj.; (f) 20 μM **8**, + *hv*, 100X obj. (zoomed).

of a successful photochemotherapy agent. Importantly, the photocytotoxicity associated with the dyads results in apoptosis, which is a necessary consideration in the development of new molecules for clinical purposes. Together, the findings reported herein introduce supramolecular systems derived from conjugated Ru(II)-diimine dyads as promising candidates to be included in the arsenal of potential photochemotherapeutic agents under investigation.

Acknowledgment. S.A.M., S.M., J.S., and R.L. thank the Natural Sciences and Engineering Research Council of Canada, the Canadian Foundation for Innovation, and the Nova Scotia Health Research Foundation for financial support and Prof. Todd Smith for invaluable help with cell culture protocols. A.C., R.Z., and R.P.T. thank the Robert A. Welch Foundation (E-621) and the National Science Foundation (CHE-0714751) for financial support.